THE JOURNAL OF PHYSICAL CHEMISTRY C

Article

pubs.acs.org/JPCC

Computational Design of Porous Graphenes for Alkane Isomer Separation

Liying Zhang,[†] Chao Wu,[*,†,‡] Yong Fang,[†] Xiangdong Ding,[*,†] and Jun Sun[†]

[†]State Key Laboratory for Mechanical Behavior of Materials and [‡]Frontier Institute of Science and Technology, Xi'an Jiaotong University, Xi'an 710049, People's Republic of China

Supporting Information

ABSTRACT: Using first-principles calculations, we systematically evaluated a series of single-layer porous graphene membranes with different sized pores passivated by hydrogen atoms for separating short alkane isomers (C = 5−7). We found that graphene membranes with appropriate pore size (e.g., the *pore19* model whose pore size is 8.0 × 5.8 Å) could efficiently separate dibranched isomers from their monobranched and linear counterparts. When alkane molecules diffused through a membrane, the porous graphene might exhibit significant distortion. At the same time, the passing molecule would be forced to change its own geometry as well. More importantly, we found that the geometric deformations of both the penetrating molecule and the membrane concertedly lowered the diffusion barrier by similar magnitudes. Therefore, when designing two-dimensional (2D) separation materials, it is necessary to consider the geometric flexibility of both the separation material and the molecules to be separated. Our results theoretically verified the feasibility of utilizing porous graphene and possibly other 2D materials for screening alkane isomers, which could lead to a wide range of energy and environment related applications.

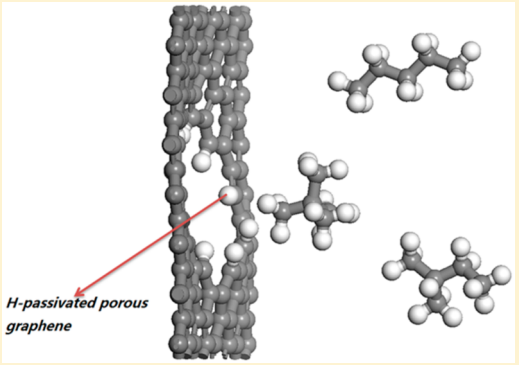

1. INTRODUCTION

It is always a hard question how to separate molecules with close physical properties, yet efficient separation is crucial for chemical, petrochemical,[1−3] and environmental-related industries.[4,5] Porous structures, especially ordered crystalline nanoporous materials, are often considered as separation media. Zeolites and zeolitic imidazolate frameworks (ZIFs),[6,7] metal−organic frameworks (MOFs),[8−10] covalent organic frameworks (COFs),[11,12] etc., all have been tested for separating the notorious alkane mixtures composed of linear, monobranched, and dibranched isomers, whose separation is solely dependent on their geometry difference.

However, these porous structures typically have thickness ranging from tens of nanometers to several micrometers. As thickness is inversely proportional to a material's permeance, such thickness may limit the overall separation efficiency of the materials. Two-dimensional (2D) materials represented by graphene may overcome this problem as they are essentially only one- or few-atom thick membranes.[13] Additionally, a number of 2D materials have shown considerable mechanical strength and chemical stability; therefore, they have been proposed as potential optimal separation materials.[14−17] Nevertheless, perfect 2D membranes, such as monolayer graphene sheets, are impermeable even to the smallest gas of He.[18,19] Naturally, people have explored the possibility of utilizing *porous* 2D materials for separation. If the uniformity of size and distribution of pores can be achieved, then the separation performance of porous 2D membranes solely depends on the pore properties, which can be tailored by changing the size, shape, and passivating elements of the pores.[20]

Initially, graphene with small pores has been theoretically evaluated for separating gas molecules, whose kinetic diameters are usually ∼3 Å. Through molecular dynamics (MD) simulations and density functional theory (DFT) calculations, it has been shown that small-molecule mixtures like H_2/N_2,[21] H_2/CH_4,[22] and CO_2/N_2[23] can be well separated by porous graphene with proper pore size and passivation. Particularly, by using MD simulations, Nieszporek et al. studied the permeability of a methane/butane mixture passed through H-passivated porous graphene sheets with pore diameters of 3.2 Å, whose high selectivity was found to be governed by the volume exclusion mechanism.[24] Cohen and Grossman in their seminal paper theoretically demonstrated that the single-layer graphene with hydrogenated and hydroxylated nanometer-scale pores could be used as an effective membrane for water desalination.[25] Salt ions are pretty much screened by pores smaller than 8 Å of diameter, while the water permeability is several orders of magnitude higher than those of conventional reverse osmosis membranes.[26]

Experimentally, various ways to introduce closely spaced nanopores into graphene sheets have been developed, including beam treatment, heavy ion bombardment, oxidative etching,

Received: March 27, 2017
Published: April 17, 2017

DOI: 10.1021/acs.jpcc.7b02915
J. Phys. Chem. C 2017, 121, 10063−10070

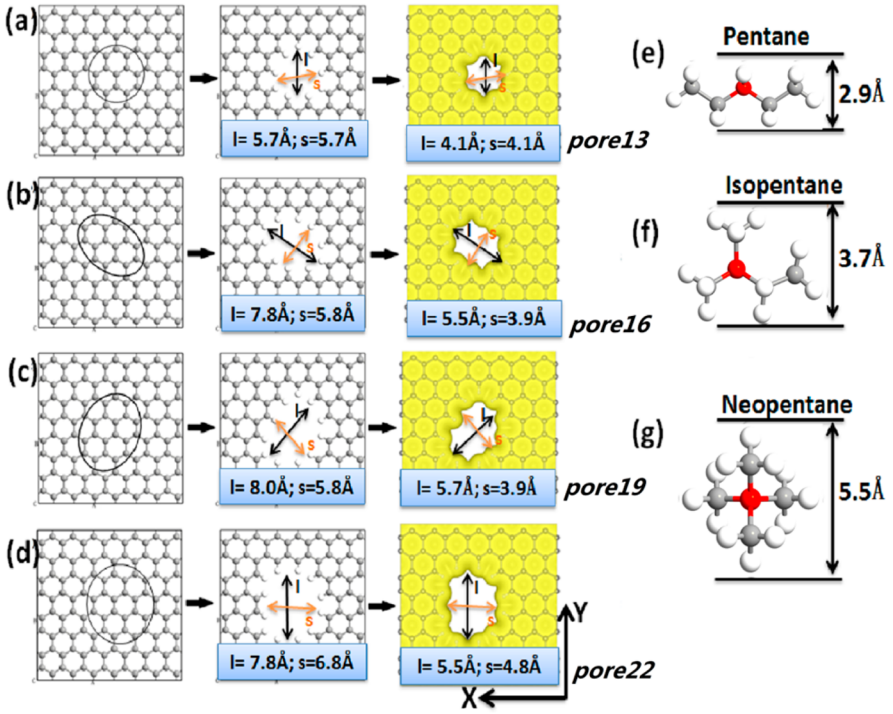

Figure 1. Models of the H-passivated porous graphene membranes and the passing molecules: (a) *pore13*, (b) *pore16*, (c) *pore19*, and (d) *pore22*. Left panel: black circles highlight the regions where carbons were removed. Middle panel: geometric pore size. Right panel: pore size according to electron density (isovalue 0.02 e/Å^3). *s* and *l*, respectively, label the shortest and the longest diameters of a pore. Pentane isomers labeled with their minimum geometric diameters: (e) pentane, (f) isopentane, and (g) neopentane. Gray balls: carbon. White balls: hydrogen. Red dots: carbon atoms used to calculate the distance (adsorption height) between the molecule and membrane.

graphene oxide reduction, or chemical synthesis.[27−29] For example, Wang et al. used a metalized atomic force microscope (AFM) tip to punch sparse and discrete angstrom-sized holes (diameters about 300 nm) in monolayer graphene sheets. They later successfully placed gold nanoparticles on the graphene sheets and were able to precisely manipulate the relative particle-hole positions by laser beams which can activate thermo motion of the nanoparticles. Consequently, the gas flux through the porous graphenes can be regulated by these gold nanovalves.[30] Meanwhile, Celeb et al. used the heavy ion bombardment method to drill evenly distributed pores with nearly uniform pore sizes, which can be controlled from less than 10 nm to 1 mm.[31] Still, most experimental methods can only make graphene with pore size larger than 7 nm in large quantity,[32] which is much larger than the above-discussed gas molecules.

However, this pore size may be suitable for separating larger molecules, such as isomers of alkanes with 5−7 carbons, which are relevant to gasoline production. Herm et al. reported the syntheses of a series of highly stable MOFs with triangular channels with diameters of about 7 nm, which can separate hexane isomers according to the degree of branching.[2] Dubbeldam et al. showed by simulation that ZIF-77 (the limiting diameter of about 9.3 nm) had a significantly higher selectivity for separating dibranched alkanes from their isomers, i.e., by about 2 orders of magnitude over current materials in use.[1] The separation performance of porous materials like MOFs and ZIFs discussed above is mainly determined by the pore size. Thus, here we carried out a systematic first-principles study to explore the performance of porous graphene membranes with pore diameters larger than 5 nm for alkane isomer separation. To simplify our discussion, the unsaturated carbon atoms at the pore edges are H-passivated,[33] as H-ion bombardment is one way to prepare porous graphene.[34] We first designed four porous graphene models with different pore sizes and shapes. Then we studied the diffusion potential energy surfaces of the three pentane isomers. Next, we evaluated the selectivity and identified the best separation model. Later, we quantitatively analyzed the geometric deformation during penetration for both the isomers and the porous graphene models. Further, we checked the performance of the best model for separating other alkane isomers (C6 and C7). Finally, we discussed and concluded the principles for designing porous graphene-like 2D separation materials.

2. METHODS

The geometry optimizations and property calculations were performed by using first-principles methods, which is a combination of DFT and the nonequilibrium Green's function (NEGF) technique as implemented in the Atomistix ToolKit (ATK).[35,36] The generalized gradient approximation (GGA) using the Perdew−Burke−Ernzerhof (PBE) functional[37] was employed for describing the exchange−correlation interactions. The wave functions were expanded by using a double-ζ (DZ) basis for H atoms and double-ζ plus polarization (DZP) bases for other atoms. The Monkhorst−Pack *k*-point mesh was chosen to be 4 × 4 × 1 in the *x*, *y*, and *z* directions, respectively, and the related energy cutoff was set to be 75 hartree. For all models, a 20 Å vacuum was introduced to minimize image interactions. After optimization, all residual forces on each atom are smaller than 0.05 eV/Å. The minimum energy paths for molecules diffusing through the pores were calculated using the nudged elastic band (NEB) method.

DOI: 10.1021/acs.jpcc.7b02915
J. Phys. Chem. C 2017, 121, 10063−10070

The interaction energy between a passing molecule and the porous graphene model is defined as follows

$$E_{int} = E(\text{total}) - E(\text{pore}) - E(\text{molecule}) \quad (1)$$

where E(total) is the energy of the molecule−porous graphene complex. E(pore) and E(molecule) are the energies of the porous graphene and the passing molecule, respectively. If E_{int} is less than zero, the interaction is exothermic. Following previous studies,[38,39] the initial state (IS) and the final state (FS) feature perpendicular configuration of the molecule with respect to the graphene plane.

The diffusion energy barrier is defined as

$$E_b = E_{TS} - E_{ref} \quad (2)$$

where E_{TS} and E_{ref} represent the energy of the transition state (TS, the highest point on the potential energy surface) and the reference state E_{ref} (the distance between the molecule and the graphene plane is 6 Å).

Our calculation setup was tested by reproducing literature values, where porous graphenes were used to separate small molecules like CH_4, H_2, and N_2.[22,38] We found that the diffusion energetics obtained by single-point energy calculations are quantitatively close to the literature values (difference in barriers <0.15 eV; for details, see Supporting Information, Figure S1). However, the barrier obtained by single-point calculations is lowered substantially by the NEB method (e.g., the barrier is lowered by ∼1.2 eV for CH_4), which was not reported in the compared literature.[22,38] We also checked the dispersion interaction between the CH_4 and porous graphene with the DFT-D2 method (Figure S 1d).[40] Again, the results agreed with the reported values quite well, and the barrier was close to the results of the functional without van der Waals forces. Therefore, to save computational cost, we did not consider dispersion interactions in the following calculations. Moreover, we tested the influence of the size of porous graphenes (e.g., *pore19*, in Figure S2). By increasing the size of the graphene sheet by half and keeping the pore size unchanged, we observed the same barrier for neopentane penetration.

3. RESULTS AND DISCUSSION

3.1. Models of Porous Graphene Membranes. We proposed four models with different pore size and shape, named after the number of deleted C atoms: *pore13*, *pore16*, *pore19*, and *pore22* (Figure 1), whose unsaturated carbons are passivated by H atoms. The pore size according to geometry and the electron density isosurface are characterized by the shortest (s) and longest (l) distances between atoms and electron density isosurface, respectively.[22] It is worth noting that the pore size characterized by the electron density isosurface may serve as an auxiliary parameter in addition to the geometric diameter, as the penetration requires extra distance to avoid overlapping the electron clouds between the atoms of the molecule and the pore. All the pores are approximately round or ellipsoidal with geometric diameters comparable to or larger than the isomers. The distance between the passing molecule (the red carbon atom) and the porous graphene plane is defined as the adsorption height. At the adsorption height of ±6 Å, the interaction between the passing molecules and the porous graphene is close to zero, which is the effective interaction range considered in the calculations.

3.2. Diffusion Barrier and Selectivity. We computed diffusion energetics of three pentane isomers passing through the four porous graphene models using the NEB method (Figure 2). Naturally, the energy barrier reduces with the

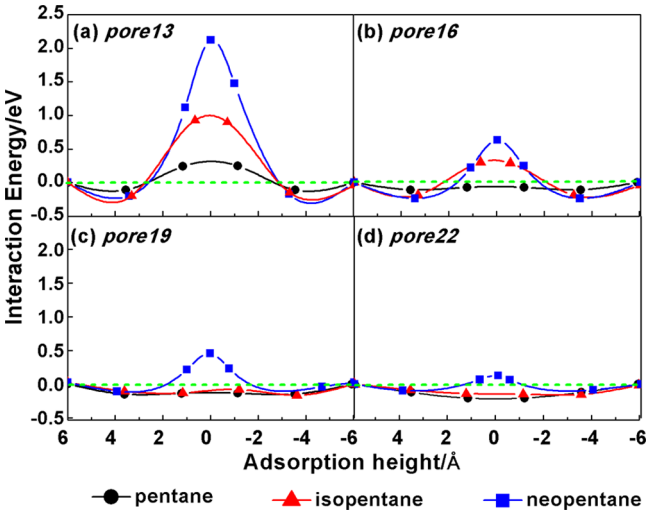

Figure 2. Diffusion energetics of pentane isomers penetrating porous graphene membranes. (a) *pore13*, (b) *pore16*, (c) *pore19*, and (d) *pore22*. Filled symbols are the values obtained from the actual NEB images.

increasing pore size. There is no evident barrier for all three isomers passing through *pore22*, while for *pore19*, only neopentane shows a moderate barrier of ∼0.5 eV. For *pore16*, both neopentane and isopentane experience small to moderate barriers of ∼0.3 and 0.6 eV, respectively. Pore size between *pore16* (geometric l = 7.8 Å and s = 5.8 Å) and *pore19* (geometric l = 8.0 Å and s = 5.8 Å) seems to be able to efficiently separate the dibranched pentane molecules (geometric diameter = 5.5 Å) from other isomers. All three pentane isomers have to overcome barriers when passing through *pore13* (geometric l = 5.7 Å and s = 5.7 Å), and correspondingly the barriers are 2.1, 1.0, and 0.3 eV for neopentane, isopentane, and pentane. As a result, neopentane is blocked completely, and isopentane (geometric diameter = 3.7 Å) begins to suffer high barrier, leaving only pentane practically penetrable. The difference in barriers increases significantly when the pore's longest diameter is comparable to the size of the passing molecule. In contrast, when the pore's longest diameter increases from 7.8 Å in *pore16* to 8.0 Å in *pore19*, both of which are already much larger than the diameter of the molecule, the barrier of neopentane is reduced slightly by 0.2 eV.

If the two geometric diameters (s and l) of the pores are averaged, a simple correlation pattern between the average pore size and the energy barrier can be observed (Figure 3a). As the average pore size becomes larger, the energy barrier reduces until it reaches zero. Clearly, the zero-barrier diameter for pentane, isopentane, and neopentane increases from 6.8 to 6.9 and then to 7.3 Å, correspondingly. As these critical diameters for pentane and isopentane are close, the right pore size range between 6.8 and 7.0 Å should be the target for separating the dibranched C5 isomers from their monobranched and linear counterparts. Naturally, as the barrier drops, the distance between the passing molecule and the pore rim is observed to become larger (Figure 3b). When the barrier and the minimum distance (d_{min}) are plotted together (Figure 3c), we can see that the critical d_{min} for zero-barrier for pentane and isopentane are

DOI: 10.1021/acs.jpcc.7b02915
J. Phys. Chem. C 2017, 121, 10063−10070

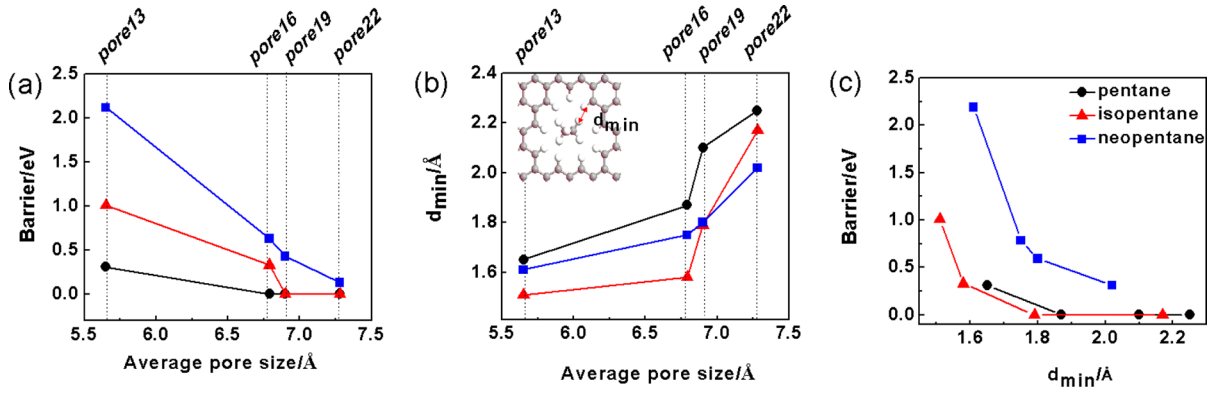

Figure 3. Penetration barrier and geometric parameters. (a) The energy barrier versus the average pore size. (b) The minimum distance versus average pore size. d_{min} is defined in inset, the distance between two hydrogen atoms. (c) The minimum distance versus barrier.

close again but with isopentane's d_{min} being smaller (1.8 vs 1.9 Å for isopentane and pentane, respectively). This may be an artifact that *pore16* could be a little bit larger than the minimum pore for pentane to have zero barrier. Evidently, different passing molecules may have different zero-barrier d_{min}, which effectively combines the information on the pore shape and size as well as the size of the molecule. Therefore, d_{min} may serve as a more general guiding parameter for designing separation materials.

Table 1. Energy Barrier and Selectivity of Pentane Isomers Passing through Different Porous Graphene Membranes

barrier/eV	*pore13*	*pore16*	*pore19*	*pore22*
pentane	0.31	0	0	0
isopentane	1.01	0.33	0	0
neopetane	2.12	0.63	0.43	0.13
selectivity S_P:S_I:S_N	10^{30}:10^{18}:1	10^{10}:10^{5}:1	10^{7}:1:1	10^{3}:1:1

With the barriers at hand, we were able to compute the relative selectivity (S, Table 1) for the porous graphene models, using the Arrhenius equation for diffusion.

$$S_{P/I} = \frac{D_P}{D_I} = \frac{A_P}{A_I}\frac{e^{-E_P/RT}}{e^{-E_I/RT}} \quad (3)$$

where D, A, and E are diffusion rate, prefactor, and diffusion barrier, respectively. It is well-known that the prefactor A is hard to get, as the real values can only be obtained either by experimental measurements or through molecular dynamics simulations. For a 0th order of approximation, we assumed the collision frequencies in the correct orientation (frequencies of attempts to penetrate) are the same for the pentane isomers, i.e., $A_P/A_I \approx 1$, and we chose room temperature (T = 300 K).[22,41,42]

The selectivity of pentane isomers passing through *pore13* is 10^{30}:10^{18}:1 for pentane, isopentane, and neopentane, which is very high compared with that of similar systems targeting small gas molecule separation.[20] However, the energy barriers are also large, which can lead to low overall permeability. So *pore13* may not be ideal for separating pentane isomers. The selectivity of *pore22* is 10^{3}:1:1; however, the small barrier (0.13 eV) of neopentane may be further washed out by thermo fluctuation. The selectivities of *pore19* and *pore16* are in the middle. Considering the moderate barrier of about 0.5 eV, they may be the best choice for separating neopentane molecules from other isomers.

3.3. Geometric Deformation Analysis. During the penetration of the pentane isomers, we found that both the passing molecule and the porous graphene deform evidently. Snapshots of pentane isomers passing through *pore13* at the adsorption heights from −2 to 4 Å are shown in Figure 4a–c. The substrate exhibits slight bulging as the pentane permeates *pore13*. When isopentane and neopentane diffuse through, *pore13* presents substantial out-of-plane deformation, especially in the scope of −1 to 1 Å. In contrast, it is hard to visualize the deformation of the isomers directly. Quantitative analysis was carried out by comparing the isolated structure with the one experiencing penetration. The out-of-plane deformation of the rim atoms ($d|\bar{z}|$, averaged deformation in z-axis, Figure 4d–f) was our concern for analyzing the porous graphene (details, see SI Figure S2), while for isomers, we compared the positions of all the atoms ($d|\bar{g}|$, averaged change of atomic positions, Figure 4g–i). The biggest out-of-plane deformations for pentane, isopentane, and neopentane are correspondingly 0.015, 0.022, and 0.025 Å. For neopentane, this happens at the adsorption height at 1 Å rather than at 0 Å for the other two isomers. By combining the highly unsymmetrical geometric deformation snapshots, we can conclude that the penetration of neopentane is much like squeezing an oversize item through a soft door.

Meanwhile, the energy variation due to the geometry change was computed and plotted. For pentane, the slight deformation of *pore13* does not generate appreciable energy rise. Moderate (0.35 eV) and large (0.70 eV) energy increases are observed for isopentane and neopentane, correspondingly. This suggests that the porous graphene is flexible; however, if the distortion goes beyond certain limits (here $d|\bar{z}|$ = 0.02 Å) the energy penalty comes into play. The analyses of molecules in general show less evident deformation (<0.01 Å/atom), which implies that they are much more rigid than graphene. Additionally the biggest distortion always takes place before the molecule reaches the energy barrier position, suggesting the molecules are "squeezed" before passing through the pore. More importantly, the increase in terms of the molecule's energy due to its distortion for isopentane and neopentane is about 0.25 and 0.40 eV, respectively. Though the numbers are lower than the energy change caused by the graphene deformation, they are far from negligible. As a consequence, both the geometry distortions and their corresponding energy changes should be taken into consideration when evaluating the separation performance. For example, the total energy change

DOI: 10.1021/acs.jpcc.7b02915
J. Phys. Chem. C 2017, 121, 10063−10070

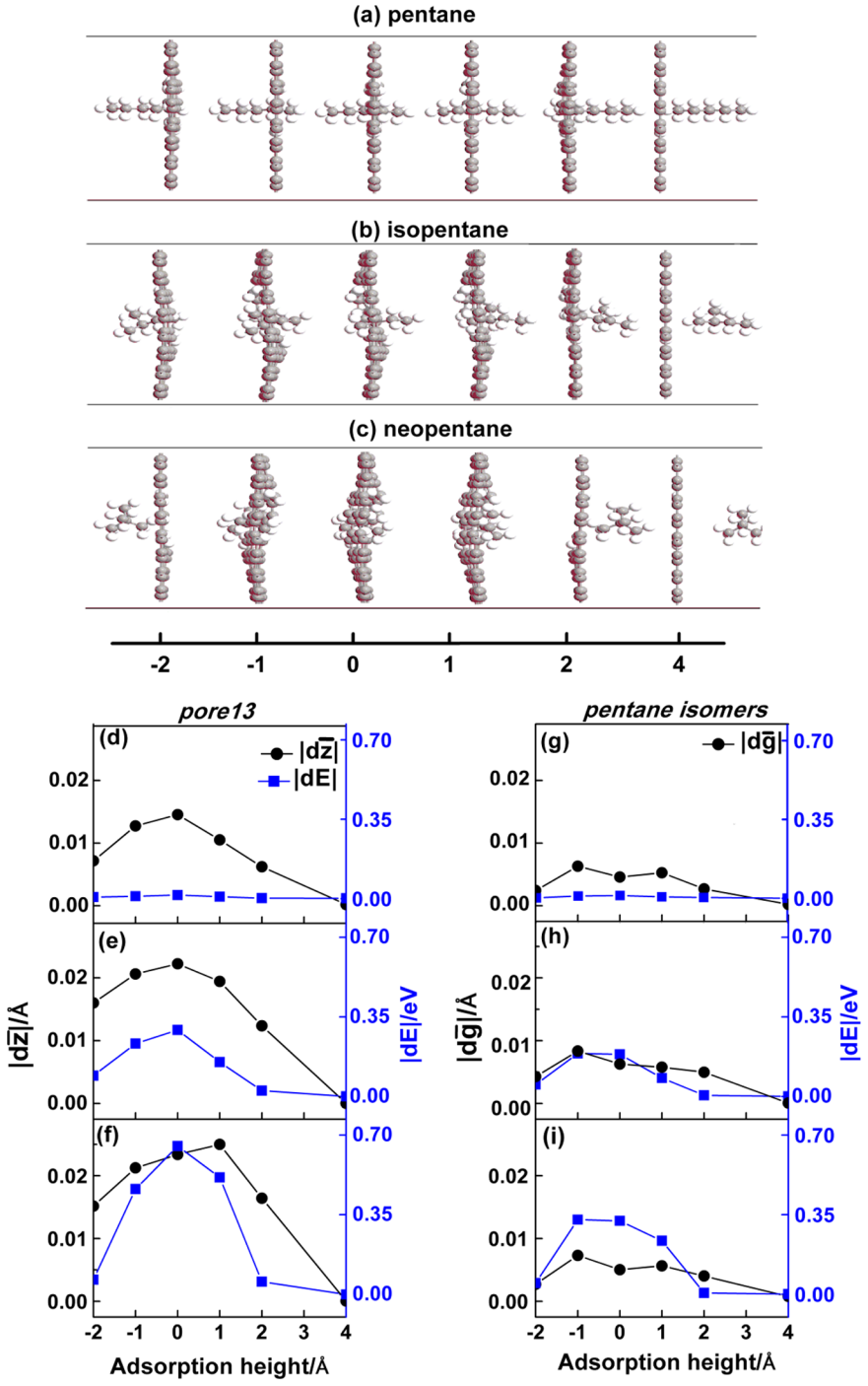

Figure 4. Typical penetration process. Snapshots of pentane isomers passing through *pore13*: (a) pentane, (b) isopentane, and (c) neopentane. The *z*-direction deformation ($d|\bar{z}|$) and the energy change ($|dE|$) of *pore13* due to the isomers: (d) pentane, (e) isopentane, and (f) neopentane. The atomic displacement ($d|\bar{g}|$) and the energy change ($|dE|$) of the isomers during penetration: (g) pentane, (h) isopentane, and (i) neopentane.

($|dE|$ due to deformation of *pore13* (0.65 eV) and neopentane (0.32 eV)) is 0.97 eV, and it accounts for almost 50% of the energy barrier (2.12 eV).

We further analyzed the geometric distortion and the corresponding energy change when the pentane isomers diffuse through other porous graphene models. Only the changes at the adsorption height of 0 Å during penetration are presented (Figure 5). Obviously, the energy change ($|dE|$) and the deformation ($d|\bar{z}|$ and $d|\bar{g}|$) decrease with the increasing pore size (for snapshots of isomers diffusing through other models, see SI Figures S3 and S4). The energy and geometry changes of the isomers are much smaller than that of the porous graphenes, which reflect their higher rigidity. Among the isomers, neopentane has the highest rigidity as it exhibits the least deformation when penetrating smaller pores like *pore13* and *pore16*, while its energy change is bigger than the other two (Figure 5d). For example, $d|\bar{g}|$ of neopentane is 0.005 Å during passing *pore13* and is 0.003 Å in *pore22*, which is probably due to its bulky size and short chain length (Figure 5c). In comparison, the longer chain of pentane and structural asymmetric structure of isopentane result in bigger deformations of 0.007 and 0.006 Å in *pore13*, respectively.

DOI: 10.1021/acs.jpcc.7b02915
J. Phys. Chem. C 2017, 121, 10063−10070

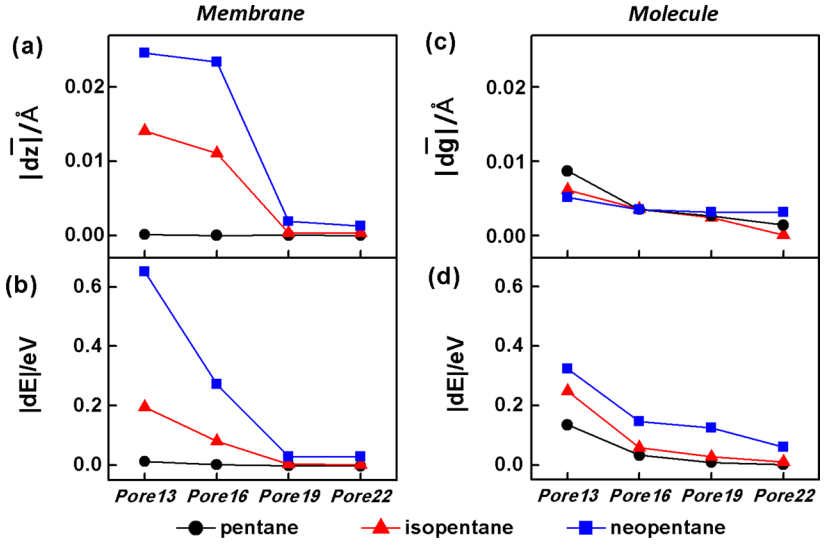

Figure 5. Analysis at the point of penetration. Analysis is carried out at the adsorption height of 0 Å. (a) Structural deformation of the porous graphene membranes. (b) Energy change of the porous graphene membranes due to the structural deformation. (c) Structural deformation of pentane isomers. (d) Energy change of pentane isomers due to the structural deformation. As the guide to the eye, lines of the same color link the data of the same diffusing molecule.

3.4. Relaxed versus Unrelaxed Structures. So far, most studies about small molecule separation assumed rigid structures for calculating the diffusion barrier and had not considered the impact of structure relaxation and its consequences on the barrier and selectivity.[25,26,43−45] Few works did consider the effect of the deformation of porous graphenes. Hauser et al.[46] used functionalized nanoporous graphenes to efficiently separate methane from air. The energy barrier of CH_4 drops from 0.94 eV before structure relaxation to 0.35 eV after relaxation. Correspondingly, the selectivity of air over CH_4 is greatly reduced from 10^{18}:1 to 10^{7}:1. The significant influence of the structure of the porous graphene on energy barrier and selectivity has been well documented. However, the contribution from the molecular deformation seems to be missing.

As we have shown that the structure change is closely linked to the potential energy surface of diffusion, we further directly compared the diffusion energetics of the NEB calculations (which allow the structure to relax) to the single-point calculations (which use rigid or unrelaxed structures obtained by interpolation or extrapolation of the structures of initial and/or final states). We used neopentane as an example to show how its diffusion barrier changes when passing different graphene models (Figure 6). The energy barriers of NEB calculations are significantly lower than that of single-point calculations when the size of the passing molecule is close to the size of the pore. For example, for neopentane passing through *pore13*, the unrelaxed and relaxed barriers are 7.9 and 2.1 eV, respectively, a drop over 3/4. For bigger pores like *pore19* and *pore22*, the results from two methods are much closer. Similarly, for pentane, its barriers for passing through all four graphene models are small no matter the structures are allowed to relax or not. For example, when diffusing through *pore13*, its barriers are 0.5 and 0.3 eV for rigid and relaxed calculations, respectively. Consequently, the selectivity of the isomers varies significantly (by many orders of magnitude) between the two kinds of calculations (Table 1 and SI, Table S1), with the unrelaxed calculations of higher selectivity.[38]

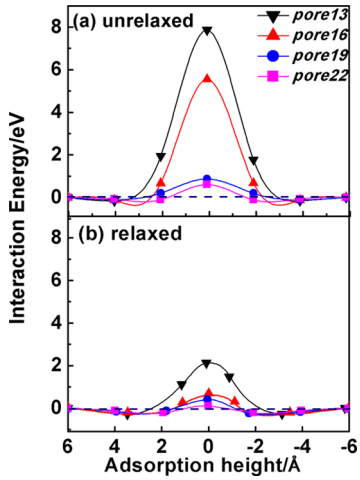

Figure 6. Unrelaxed calculations versus relaxed calculations. The diffusion energetics of neopentane passing through four porous graphene models are plotted as a function of the adsorption height. (a) Calculations using unrelaxed structures. (b) Calculations using relaxed structures.

3.5. Effect of Chain Length. We have shown that porous graphene with proper pore size should be able to separate pentane isomers; however, in the gasoline industry, in addition to C5, alkanes like hexane and heptane are equally important, and the separation of their isomers is also crucial. We used *pore19*, the model with the highest selectivity for C5 separation, to check whether longer chains affect the separation performance or not (Figure 7). Virtually the same as C5, there is no barrier for linear and monobranched C6 and C7, and the barrier for dibranched C5 remains for dibranched C6 and C7. So chain length does not affect the selectivity of the porous graphene, which suggests that porous graphene sheets similar to *pore19* are a promising candidate for separating short-chain alkane isomers.

Additionally, it is worth noting that there may be a "cork effect" due to the stable adsorption state of some of the molecules in the mixture to be separated, which will block the

DOI: 10.1021/acs.jpcc.7b02915
J. Phys. Chem. C 2017, 121, 10063−10070

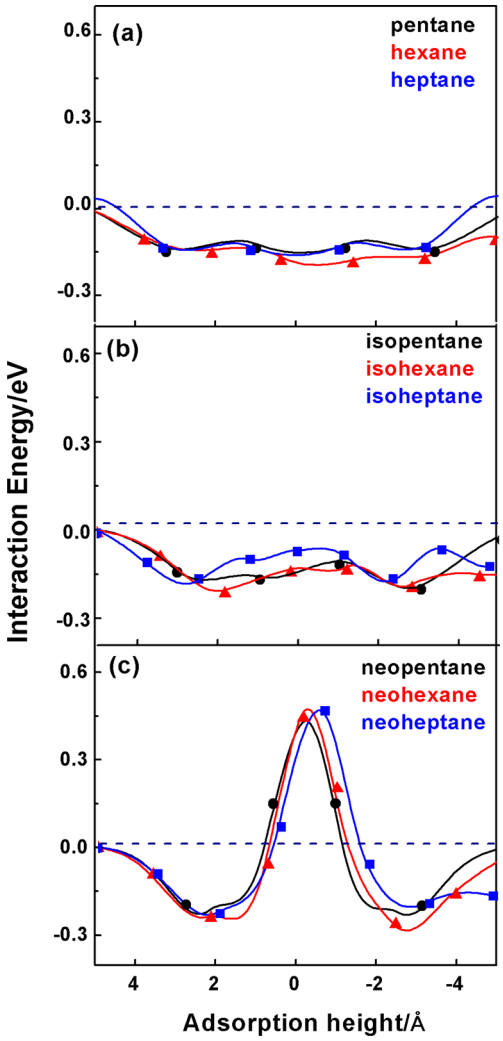

Figure 7. Chain length effect. The interaction energy between alkane isomers and *pore19* as a function of adsorption height is plotted. (a) Linear isomers of C5, C6, and C7. (b) Monobranched isomers of C5, C6, and C7. (c) Dibranched alkanes isomers of C5, C6, and C7. Nearly overlapped curves imply the separation performance is insensitive to the carbon number.

pore.[24] To have this effect, the blocking molecule needs to have a negative free energy of adsorption, which requires a very strong interaction (negative adsorption energy) to overcome the entropy loss of the molecule when it attaches to the pore. The estimated translational entropy loss of pentane isomers based on the ideal gas model is about 1.0 eV at room temperature,[47] which means that the interaction energy between pentane isomers and the pore needs to be lower than −1.0 eV, while the actual interaction energies are all higher than −0.3 eV. Although the cork effect is not evident in our system, by changing the passivating element in the pore rim, the interaction between the gas molecule and the pore may be enhanced to block the pore. Actually, this blocking mechanism may be utilized as a dynamic way or a gate to regulate the pore size.

4. CONCLUSIONS

We have computationally evaluated the performance of four single-layer porous graphene membrane models for separating isomers of short alkanes including C5∼C7, whose minimum geometric diameters range from 2.9 to 5.5 Å. Our results show that H-passivated porous graphene models can separate linear and monobranched alkanes from their dibranched counterparts. Particularly, the *pore19* model, where 19 carbon atoms are taken out from the graphene sheet leaving an ellipsoidal pore of the size of 8.0 × 5.8 Å, exhibits a high selectivity for linear and monobranched isomers over the dibranched ones at the ratio of 10^7:1. Simultaneously, a high overall permeability is implied by the moderate barriers, i.e., 0.5 eV, for dibranched C5∼C7 isomers and 0 eV for other isomers. We found that calculations allowing the structure to relax produce much lower penetration barriers than calculations that do not, which is crucial in estimating permeability and separation selectivity. Our work should be useful for designing advanced 2D membranes for alkane isomer separation.

■ ASSOCIATED CONTENT

Supporting Information

The Supporting Information is available free of charge on the ACS Publications website at DOI: 10.1021/acs.jpcc.7b02915.

Figure S1, The diffusion energetics of molecules penetrating *pore10*. Figure S2, the barrier and size of porous graphenes. Figure S3, Atoms used for calculating the graphene distortion. Figure S4, Deformation analysis of neopentane passing through *pore16*. Figure S5, Deformation analysis of pentane isomers passing through *pore19*. Table S1, energy barrier and selectivity of pentane isomers pass through the different porous graphene membranes using unrelaxed (rigid) structures (PDF)

■ AUTHOR INFORMATION

Corresponding Authors

*E-mail: chaowu@mail.xjtu.edu.cn.
*E-mail: dingxd@mail.xjtu.edu.cn.

ORCID

Chao Wu: 0000-0002-8573-7196

Notes

The authors declare no competing financial interest.

■ ACKNOWLEDGMENTS

This work was supported by the National Natural Science Foundation of China (Nos. 51320105014, 51621063, 21477096).

■ REFERENCES

(1) Dubbeldam, D.; Krishna, R.; Calero, S.; Yazaydin, A. O. Computer-assisted screening of ordered crystalline nanoporous adsorbents for separation of alkane isomers. *Angew. Chem., Int. Ed.* **2012**, *51*, 11867−11871.

(2) Herm, Z. R.; Wiers, B. M.; Mason, J. A.; van Baten, J. M.; Hudson, M. R.; et al. Seperation of hexane isomers in a metal-organic framwork withtriangular channels. *Science* **2013**, *340*, 960−964.

(3) Vermeiren, W.; Gilson, J.-P. Impact of zeolites on the petroleum and petrochemical industry. *Top. Catal.* **2009**, *52*, 1131−1161.

(4) Elimelech, M.; Phillip, W. A. The Future of Seawater Desalination: Energy, Technology, and the Environment. *Science* **2011**, *333*, 712−717.

(5) Hillie, T.; Hlophe, M. Nanotechnology and the challenge of clean water. *Nat. Nanotechnol.* **2007**, *2*, 663−664.

(6) Banerjee, R.; Furukawa, H.; Britt, D.; Knobler, C.; et al. Control of pore size and functionality in isoreticular zeolitic imidazolate. *J. Am. Chem. Soc.* **2009**, *131*, 3875−3877.

DOI: 10.1021/acs.jpcc.7b02915
J. Phys. Chem. C 2017, 121, 10063−10070

(7) Galvelis, R.; Slater, B.; Cheetham, A. K.; Mellot-Draznieks, C. Comparison of the relative stability of zinc and lithium-boron zeolitic imidazolate frameworks. *CrystEngComm* **2012**, *14*, 374−378.
(8) Eddaoudi, M.; Kim, J.; Rosi, N.; Vodak, D.; Wachter, J.; O'Keeffe, M.; Yaghi, O. M. Systematic design of pore size and functionality in isoreticular MOFs and their application in methane storage. *Science* **2002**, *295*, 469−472.
(9) Yaghi, O. M.; O'Keeffe, M.; Ockwig, N. W. Reticular synthesis and the design of new materials. *Nature* **2003**, *423*, 705−714.
(10) Dybtsev, D. N.; Chun, H.; Kim, K. Rigid and flexible: a highly porous metal−organic framework with unusual guest-dependent dynamicbehavior. *Angew. Chem.* **2004**, *116*, 5143−5146.
(11) Côté, A. P.; Benin, A. I.; Ockwig, N. W.; O'keeffe, M. Porous, crystalline, covalent organic frameworks. *Science* **2005**, *310*, 1166−1170.
(12) El-Kaderi, H. M.; Hunt, J. R.; Mendoza-Cortés, J. L.; et al. Designed synthesis of 3D covalent organic frameworks. *Science* **2007**, *316*, 268−272.
(13) Yang, Z. Q.; Sun, Y. Q.; Alemany, L. B.; et al. Birch reduction of graphite. edge and interior functionalization by hydrogen. *J. Am. Chem. Soc.* **2012**, *134*, 18689−18694.
(14) Novoselov, K. S.; Geim, A. K.; Morozov, S. V.; Jiang, D. Electric field effect in atomically thin carbon films. *Science* **2004**, *306*, 666−669.
(15) Geim, A. K.; Novoselov, K. S. The rise of graphene. *Nat. Mater.* **2007**, *6*, 183−191.
(16) Tao, Y. H.; Xue, Q. Z.; Liu, Z. L.; Shan, M. X.; Ling, C. C.; et al. Tunable hydrogen separation in porous graphene membrane: first-principle and molecular dynamic simulation. *ACS Appl. Mater. Interfaces* **2014**, *6*, 8048−8058.
(17) Schrier, J. Fluorinated and nanoporous graphene materials as sorbents for gas separations. *ACS Appl. Mater. Interfaces* **2011**, *3*, 4451−4458.
(18) Bunch, J. S.; Vebridge, S. S.; Alden, J. S.; van der zande, A. M.; et al. Impermeable atomic members from graphene sheets. *Nano Lett.* **2008**, *8*, 2458−2462.
(19) Schrier, J. Helium separation using porous graphene members. *J. Phys. Chem. Lett.* **2010**, *1*, 2284−2287.
(20) Hu, W.; Wu, X. J.; Li, Z. Y.; Yang, J. L. Porous silicene as a hydrogen purification membrane. *Phys. Chem. Chem. Phys.* **2013**, *15*, 5753−5757.
(21) Du, H. L.; Li, J. Y.; Zhang, J.; Su, G.; Li, X. Y. Separation of hydrogen and nitrogen gases with porous graphene membrane. *J. Phys. Chem. C* **2011**, *115*, 23261−23266.
(22) Jiang, D.-e.; Cooper, V. R.; Dai, S. Porous graphene as the ultimatemembrane for gas separation. *Nano Lett.* **2009**, *9*, 4019−4024.
(23) Wu, T. T.; Xue, Q. Z.; Ling, C. C.; Shan, M. X.; Liu, Z. L.; et al. Fluorine-modified porous graphene as membrane for CO_2/N_2 separation: molecular dynamic and first-principles simulations. *J. Phys. Chem. C* **2014**, *118*, 7369−7376.
(24) Nieszporek, K.; Drach, M. Alkane separation using nanoporous graphene menbranes. *Phys. Chem. Chem. Phys.* **2015**, *17*, 1018−1024.
(25) Cohen-Tanugi, D.; Grossman, J. C. Water Desalination across Nanoporous Graphene. *Nano Lett.* **2012**, *12*, 3602−3608.
(26) Konatham, D.; Yu, J.; Ho, T. A.; Striolo, A. Simulation Insights for Graphene-Based Water Desalination Membranes. *Langmuir* **2013**, *29*, 11884−11897.
(27) Fischbein, M. D.; Drndić, M. Electron beam nanosculpting of suspended graphene sheets. *Appl. Phys. Lett.* **2008**, *93*, 113107−113110.
(28) Li, H.; Song, Z. N.; Zhang, X. J.; et al. Ultrathin, molecular-sieving graphene oxide membrane for selective hydrogen separation. *Science* **2013**, *342*, 95−98.
(29) Lu, R. F.; Meng, Z. S.; Rao, D. W.; Wang, Y. H.; Shi, Q.; et al. A promising monolar membrane for oxygen separation from harmful gases: nitrogen-substituted polyphenylene. *Nanoscale* **2014**, *6*, 9960−9964.
(30) Wang, L.; Drahushuk, L. W.; Cantley, L.; Koenig, S. P.; et al. Molecular values for controlling gas phase transport made from discrete angstrom-sized pores in graphene. *Nat. Nanotechnol.* **2015**, *10*, 785−790.
(31) Celebi, K.; Buchheim, J.; Wyss, R. M.; Droudian, A.; Gasser, P.; et al. Ultimate permeation across atomically thin porous graphene. *Science* **2014**, *344*, 289−292.
(32) O'Hern, S. C.; Boutilier, M. S. H; Idrobo, J. C.; Song, Y.; Kong, J.; Laoui, T.; Atieh, M.; Karnik, R. Selective ionic transport through tunable subnanometer pores in single-layer graphene membranes. *Nano Lett.* **2014**, *14*, 1234−41.
(33) Machado, F. B. C.; Aquino, A. J. A.; Lischka, H. The electronic states of double carbon vacancy defect in pyene: a model study for graphene. *Phys. Chem. Chem. Phys.* **2015**, *17*, 12778−12785.
(34) Xie, L. M.; Jiao, L. Y.; Dai, H. J. Selective etching of graphene edges by hydrogen plasma. *J. Am. Chem. Soc.* **2010**, *132*, 14751−14753.
(35) Brandbyge, M.; Mozos, J.-L.; Ordejón, P.; Taylor, J.; et al. Density-functional method for nonequilibrium electron transport. *Phys. Rev. B: Condens. Matter Mater. Phys.* **2002**, *65*, 165401−165417.
(36) Marchenkov, A.; Dai, Z. T.; Zhang, C. T.; Barnett, R. N.; et al. Atomic dimer shuttling and two-level conductance fluctuations in Nb nanowires. *Phys. Rev. Lett.* **2007**, *98*, 046802−046805.
(37) Perdew, J. P.; Burke, K.; Ernzerhof, M. Generalized gradient approximation made simple. *Phys. Rev. Lett.* **1996**, *77*, 3865−3868.
(38) Wang, Y.; Yang, Q. Y.; Li, J. P.; Zhong, C. L. Exploration of nanoporous graphene membranes for separating N_2 from CO_2: a muti-scale computational syudy. *Phys. Chem. Chem. Phys.* **2016**, *18*, 8352−8358.
(39) Li, D. B.; Hu, W.; Zhang, J. Q.; Shi, H.; et al. Separation of hydrogen gas from coal gas by graphene nanopores. *J. Phys. Chem. C* **2015**, *119*, 25559−25565.
(40) Berland, K.; Cooper, V. R.; Lee, K.; Schröder, E.; et al. van der Waals forces in density functional theory: a review of the vdW-DF method. *Rep. Prog. Phys.* **2015**, *78*, 066501−066541.
(41) Li, Y. F.; Zhou, Z.; Shen, P. W.; Chen, Z. F. Two-dimensional polyphenylene: experimentally available porous graphene as a hydrogen purification membrane. *Chem. Commun.* **2010**, *46*, 3672−3674.
(42) Zhang, H. Y.; He, X. J.; Zhao, M. W.; Zhang, M.; et al. Tunable hydrogen separation in $sp-sp^2$ hybridized carbon membranes: a first-principles prediction. *J. Phys. Chem. C* **2012**, *116*, 16634−16638.
(43) Surwade, P. S.; Smirnov, S. N.; Vlassiouk, I. V.; et al. Water desalination using nanoporous single-layer graphene. *Nat. Nanotechnol.* **2015**, *10*, 459−464.
(44) Wang, E. N.; Karnik, R. Water desalination: graphene cleans up water. *Nat. Nanotechnol.* **2012**, *7*, 552−554.
(45) Thomas, M.; Corry, B. A computational assessment of the permeability and salt rejection of carbon nanotube membranes and their application to water desalination. *Philos. Trans. R. Soc., A* **2016**, *374*, 1−20.
(46) Hauser, A. W.; Schwerdtfeger, P. Methane-selective nanoporous graphene membranes for gas purification. *Phys. Chem. Chem. Phys.* **2012**, *14*, 13292−13298.
(47) Atkins, P.; de Paula, J. *Atkins' Physical Chemistry*; Oxford University Press: Oxford, U.K., 2006.

DOI: 10.1021/acs.jpcc.7b02915
J. Phys. Chem. C 2017, 121, 10063−10070